# Electrostatically tunable optomechanical "zipper" cavity laser

R. Perahia, J. D. Cohen, S. Meenehan, T. P. Mayer Alegre, and O. Painter[a)]
*Thomas J. Watson, Sr., Laboratory of Applied Physics, California Institute of Technology, Pasadena, California 91125, USA*

(Received 28 June 2010; accepted 21 October 2010; published online 12 November 2010)

A tunable nanoscale "zipper" laser cavity, formed from two doubly clamped photonic crystal nanobeams, is demonstrated. Pulsed, room temperature, optically pumped lasing action at $\lambda = 1.3$ $\mu$m is observed for cavities formed in a thin membrane containing InAsP/GaInAsP quantum-wells. Metal electrodes are deposited on the ends of the nanobeams to allow for microelectromechanical actuation. Electrostatic tuning over a range of $\Delta\lambda = 20$ nm for an applied voltage amplitude of 9 V and modulation at a frequency as high as $\nu_m = 6.7$ MHz of the laser wavelength is demonstrated. © *2010 American Institute of Physics*. [doi:10.1063/1.3515296]

There has been growing interest in combining micro-optical resonators with microelectromechanical systems (MEMS) to create tunable photonic elements such as lasers, couplers, and filters.[1–3] In particular, MEMS-tunable lasers are promising for applications such as on-chip spectroscopy[4] and lightwave communication,[5] where large tunability and fast tuning speed are desirable. Additionally, as lasers and other resonant elements shrink below the micrometer scale, fabrication imperfections at the nanometer level can lead to substantial variance in the operating wavelength. The development of widely tunable optical cavities, at both the micro- and nanoscales, can benefit from recent advances in the field of cavity optomechanics in which radiation pressure forces are used to actuate and detect the motion of the cavity structure.[6] The strength of the radiation pressure force in such structures is quantified by an optomechanical coupling constant equal to the rate of change in the cavity resonance frequency $\omega$ with the amplitude of mechanical motion $x$, $g_{OM} = d\omega/dx$. In the canonical example of a Fabry–Perot, the coupling constant is proportional to the inverse of the physical cavity length. Recent theoretical and experimental work has shown that large gradient radiation pressure forces can be obtained in guided-wave nanostructures,[7–9] with effective optomechanical cavity lengths less than or equal to the wavelength of light.

Of particular interest in this work is the double nanobeam photonic crystal cavity, dubbed a zipper cavity,[9,10] in which giant radiation pressure effects have been measured. In previous work,[11] we explored theoretically the optical, mechanical, and electrostatic properties of an integrated optomechanical and MEMS zipper cavity laser, comparing all-optical radiation pressure and electrostatic actuation for laser wavelength tuning and modulation. Due to the small motional mass ($m_{eff} \sim$ pg) and large optomechanical coupling ($g_{OM} \sim 100$ GHz/nm) of the zipper cavity, wavelength tuning rates approaching $\delta\lambda/\delta x \sim 1$ nm/nm at bandwidths well over a megahertz were predicted. Here, we demonstrate such an integrated zipper cavity laser structure, formed in the InGaAsP semiconductor material system and operating in the 1300 nm wavelength band.

As shown in Fig. 1, the zipper cavity consists of a pair of nanobeams which are patterned with a linear array of holes and placed in the near-field of each other. A small chirp in the period between holes near the center of the beams is used to form localized resonant modes.[12] The predominantly transverse-electric optical modes of the two beams strongly couple and split into symmetric and antisymmetric pairs [see Fig. 1(a)], with the symmetric modes containing a large fraction of energy in the gap between the beams. The localized optical modes are strongly coupled to the in-plane mechanical motion of the beams [Fig. 1(c)], with symmetric modes tuning red and antisymmetric modes tuning blue with a reduction in the interbeam gap.

As detailed in Ref. 11, the zipper cavity geometry naturally lends itself to integration with capacitive electrome-

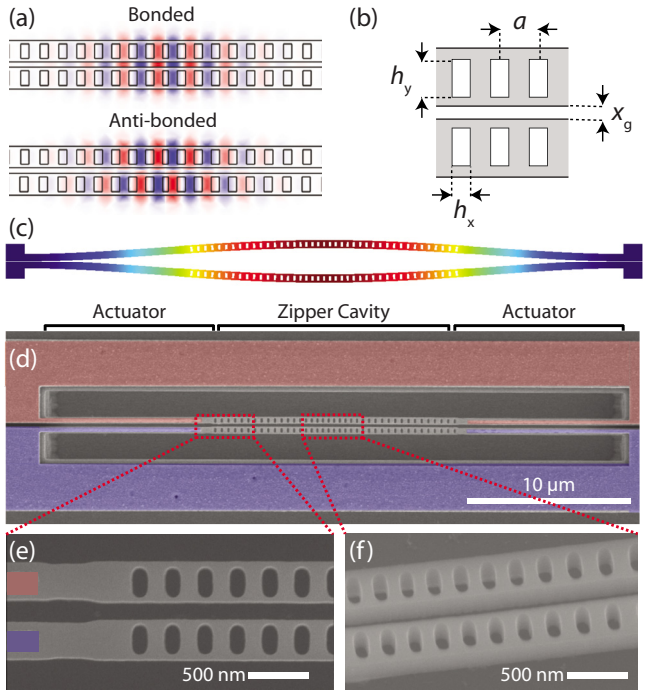


FIG. 1. (Color online) (a) FEM simulated electric field of the fundamental symmetric and antisymmetric zipper cavity modes. (b) Schematic of the zipper cavity. The designed cavity structure has an interbeam gap $x_g \approx 200$ nm, beam width $w = 417$ nm, lattice constant $a = 383$ nm, hole height $h_y = 240$ nm, and hole width $h_x = 120$ nm. (c) FEM simulated fundamental in-plane mechanical mode ($\nu_{m,1} = 1.71$ MHz, $m_{eff} = 6$ pg, $k_{eff} = 0.67$ N/m). (d) SEM micrograph of fabricated zipper cavity with positive (top) and ground (bottom) MEMS electrodes. (e) Top view of the end-mirror section and (f) angled view of the central cavity region of the zipper cavity.

[a)]Electronic mail: opainter@caltech.edu.

 

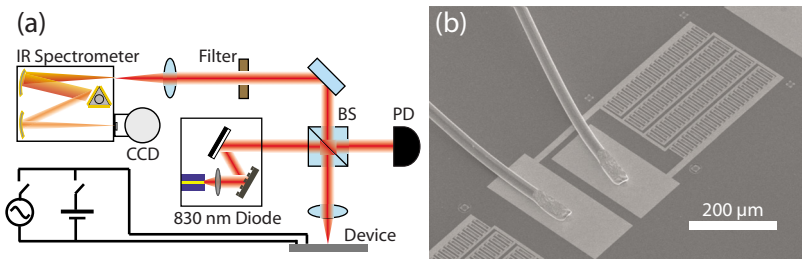


FIG. 2. (Color online) (a) Micro-PL setup with static (dc) and modulation (ac) actuation circuits. (b) SEM micrograph of a wire-bonded device array. In order to test a larger number of devices simultaneously, an array of 80 zipper cavity lasers are connected in parallel to a common pair of contacts.

chanical actuators. The zipper cavity structure studied here is fabricated from a 252 nm thick InAsP/GaInAsP multiquantum-well (MQW) layer grown on an InP substrate.[13] Fabrication of the laser cavity begins with the deposition of an insulating thin 50 nm layer of silicon nitride ($SiN_x$), followed by deposition and lift-off patterning of Ti/Au (=10/190 nm thick) metal electrodes. A second $SiN_x$ masking layer is subsequently deposited, and an aligned electron beam lithography step is used to pattern the zipper cavity nanobeams over the metal electrodes. An inductively-coupled plasma is used to etch the nanobeam pattern through the top InAsP/GaInAsP MQW layer. Finally, the zipper cavity nanobeams are released from the substrate using a hydrochloric acid wet etch[14] that selectively removes the underlying InP substrate, followed by critical point drying to avoid collapse and stiction of the beams. Scanning electron microscope (SEM) micrographs of a fabricated device are shown in Figs. 1(d)–1(f).

The devices are tested using a microphotoluminescence (micro-PL) setup shown schematically in Fig. 2(a). The devices are optically pumped with an 830 nm wavelength pulsed diode laser (pulse width $\delta T=20$ ns, pulse period $T=4$ $\mu$s). A high numerical aperture (0.4), long-working distance (32 mm) objective lens is used to focus the pump beam on the sample surface with a spot size of approximately 2 $\mu$m. PL from the sample is collected through the same objective lens, separated from the pump using a beamsplitter/interference filter combination, and then dispersed and detected by an imaging spectrometer with an attached cooled InGaAs detector array. A known fraction of the pump power is picked off by the beamsplitter and sent to a calibrated detector to estimate the power incident on the device.

A typical subthreshold PL spectrum from a zipper cavity is shown in Fig. 3(a). Several longitudinal orders of symmetric and antisymmetric cavity mode pairs are visible in the spectrum, with the lower order modes occurring at shorter wavelengths and the higher order modes at longer wavelengths. As indicated by the labeling, for each pair of modes the shorter wavelength mode is antisymmetric and the longer wavelength mode is symmetric, as confirmed by their direction of tuning in Fig. 3(a). A plot of the peak emitted power into the fundamental symmetric and antisymmetric modes versus peak absorbed pump power is shown in Fig. 3(b). A clear lasing threshold at an absorbed peak pump power of 7 $\mu$W is evident for the symmetric (1,+) mode while the emission into the antisymmetric (1, −) mode saturates above threshold due to gain (carrier) clamping. Spectra of the laser emission below, at, and above threshold are shown in Fig. 3(c). The laser linewidth narrows from $\delta\lambda\approx 0.7$ nm well below threshold to $\delta\lambda\approx 0.3$ nm at threshold, and then slowly rises to $\delta\lambda\approx 0.5$ nm well above threshold. This anomalous linewidth behavior is not atypical of micro- and nanoscale semiconductor lasers;[15] however, it is possible in these devices that the coupling of spontaneous emission fluctuations to the laser wavelength through radiation pressure may have an effect on the laser linewidth. Future experiments will seek to explore this possibility.

The wavelength tuning properties of the zipper cavity laser is tested in two different ways. First, measurements of the tuning range of the laser wavelength versus applied voltage amplitude across the capacitive electrodes is measured. Figures 4(a) and 4(b) shows the resulting laser spectra (well above threshold) from the same laser device studied in Fig. 3. The (1,+) laser mode wavelength is seen to tune red over an extended range of $\Delta\lambda=20$ nm for an applied voltage amplitude of 9 V (81 $V^2$). The (1, −) antisymmetric mode [Fig. 4(b)], on the other hand, tunes more weakly to the blue. Both modes tune in a direction corresponding to the reduction in interbeam gap with increasing voltage, as expected for the capacitor geometry. The estimated unperturbed interbeam gap from the measured symmetric/antisymmetric mode-splitting of this device is $x_g=158$ nm (consistent with SEM measurements), which from finite-element-method (FEM) simulation yields an optomechanical coupling constant of $g_+^{(1)}/2\pi=-40$ GHz/nm $(\delta\lambda/\delta x_g=0.24$ nm/nm) and $g_-^{(1)}/2\pi=26$ GHz/nm $(\delta\lambda/\delta x_g=-0.15$ nm/nm) for the (1,+) and (1, −) fundamental modes, respectively. A full numerical FEM model of the optical, mechanical, and electrostatic properties of the laser cavity structure versus applied

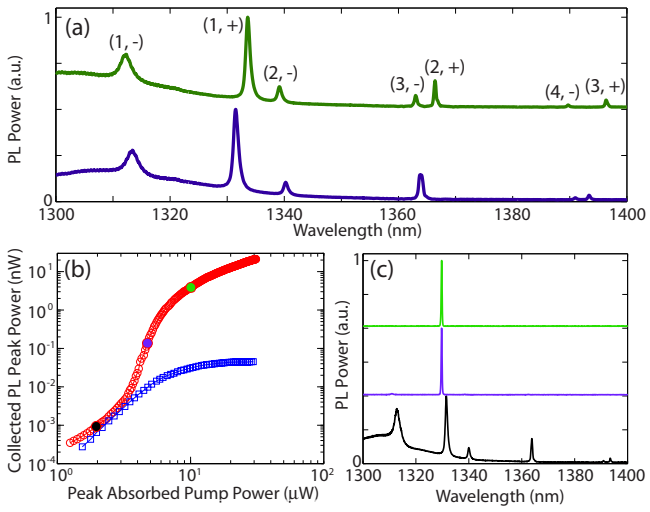


FIG. 3. (Color online) (a) Subthreshold spectrum of the optically pumped zipper cavity laser under no applied capacitor voltage (bottom curve) and a small applied capacitor voltage (top curve). (b) Light-in vs light-out (LL) curve for the fundamental symmetric (○) and antisymmetric (□) zipper cavity modes. The peak absorbed pump power is estimated from the pump duty cycle (1.1%), the fraction of the pump beam intercepted by the zipper cavity (19%), and the material absorption (10%). (c) PL spectrum below (bottom curve), at (middle curve), and above (top curve) threshold corresponding to the filled circle data points in the LL curve of (b).

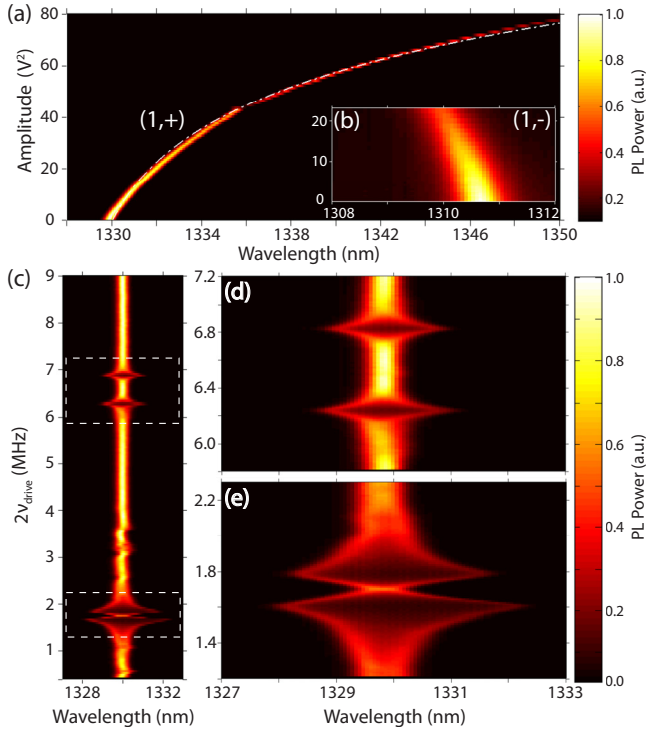


FIG. 4. (Color online) (a) PL spectra of (1,+) symmetric laser mode as a function of the applied voltage amplitude squared [Inset (b): corresponding (1, −) antisymmetric mode tuning]. A fit to the tuning curve based upon numerical FEM simulations of the laser cavity is shown as a dot-dashed white line. (c) PL spectra of the zipper cavity laser mode vs MEMS drive frequency. Zoom in of the (d) third-order and (e) first-order in-plane mechanical resonances.

voltage, taking into account the exponential dependence of the optomechanical coupling on gap distance, is shown as a white dashed-dotted line in Fig. 4(a). From this model, a shift in the nanobeam gap size of $\delta x_g^* = -20.7$ nm is inferred for the largest applied amplitude of 9 V.

A second set of tuning measurements are performed by applying a small signal voltage modulation ($\delta V_{ac}$) to the capacitive electrodes over a drive frequency range from $\nu_{drive} = 100$ to 4 MHz. The optical response of the zipper cavity to the modulated voltage input is measured by recording the time-integrated PL spectrum. The recorded spectra versus twice the drive frequency [the capacitive force scales as $(\delta V_{ac})^2$ resulting in mechanical actuation at $2\nu_{drive}$] of a laser device with a fundamental symmetric laser mode are shown in Fig. 4(b). Two resonances around $2\nu_{drive} = 1.69$ MHz and $2\nu_{drive} = 6.52$ MHz can be clearly seen in the modulation spectrum. A zoom-in around each resonance is shown in Figs. 4(c) and 4(d), indicating that each mechanical resonance is split into two frequency peaks, indicative of slight asymmetries in the two nanobeams resulting in independent beam motion. FEM mechanical simulations of the fabricated zipper cavities (nanobeam length $L = 31$ $\mu$m) yield mechanical resonance frequencies of $\nu_{m,1} = 1.71$ MHz and $\nu_{m,3} = 6.53$ MHz for the optomechanically coupled first and third order differential in-plane mechanical modes, respectively, in good correspondence with the measured resonances. Note that the second order in-plane mode is decoupled from the laser field due to its odd symmetry. From the frequency and linewidth ($\delta\nu_{m,1} \approx 150$ kHz, due to squeeze-film damping[16]) of the first order mechanical resonance, the 3 dB bandwidth and settling time for wavelength tuning of this device are estimated to be 3 MHz and 1 $\mu$s, respectively, comparable to recently demonstrated MEMS-tunable vertical-cavity surface-emitting lasers.[2]

The demonstrated wavelength tuning range (20 nm at 9 V) and wavelength modulation rate (6.7 MHz) of the zipper cavity laser can be significantly improved with a few modifications to the cavity design. A reduction in the nanobeam length of the zipper cavities to $L \approx 5$ $\mu$m should be possible, enabling a fundamental in-plane mechanical resonance frequency approaching 50 MHz, greatly enhancing the laser frequency modulation speed of the device. Reduction in the interbeam gap below 50 nm, as has been demonstrated in passive zipper cavity geometries,[17] increases the optomechanical coupling and static wavelength tuning rate of the zipper cavity modes by more than an order of magnitude. An increase in $g_{OM}$ improves not only the tunability of the cavity but also increases the radiation pressure force. Accessing a regime in which radiation pressure becomes significant, either from an external laser source or the internal laser field itself, opens up several new possibilities for all-optical laser wavelength tuning and locking.[11,16]

This work was supported by the DARPA NACHOS program (Award No. W911NF-07-1-0277). The authors would like to thank Jianxin Chen for growth of the laser material and the Kavli Nanoscience Institute at Caltech.

[1] M.-C. M. Lee and M. C. Wu, IEEE Photonics Technol. Lett. **17**, 1034 (2005).
[2] M. C. Y. Huang, Y. Zhou, and C. J. Chang-Hasnain, Nat. Photonics **2**, 180 (2008).
[3] I. W. Frank, P. B. Deotare, M. W. McCutcheon, and M. Lončar, Opt. Express **18**, 8705 (2010).
[4] F. J. Duarte, *Tunable Laser Applications*, 2nd ed. (CRC, Boca Raton, FL, 2008).
[5] C. J. Chang-Hasnain, IEEE J. Sel. Top. Quantum Electron. **6**, 978 (2000).
[6] T. J. Kippenberg and K. J. Vahala, Science **321**, 1172 (2008).
[7] M. L. Povinelli, M. Lončar, M. Ibanescu, E. J. Smythe, S. G. Johnson, F. Capasso, and J. D. Joannopoulos, Opt. Lett. **30**, 3042 (2005).
[8] M. Li, W. H. P. Pernice, and H. X. Tang, Phys. Rev. Lett. **103**, 223901 (2009).
[9] M. Eichenfield, R. Camacho, J. Chan, K. J. Vahala, and O. Painter, Nature (London) **459**, 550 (2009).
[10] P. B. Deotare, M. W. McCutcheon, I. W. Frank, M. Khan, and M. Lončar, Appl. Phys. Lett. **95**, 031102 (2009).
[11] T. P. M. Alegre, R. Perahia, and O. Painter, Opt. Express **18**, 7872 (2010).
[12] J. Chan, M. Eichenfield, R. Camacho, and O. Painter, Opt. Express **17**, 3802 (2009).
[13] W.-Y. Hwang, J. Baillargeon, S. N. G. Chu, P. F. Sciortino, and A. Y. Cho, J. Vac. Sci. Technol. B **16**, 1422 (1998).
[14] R. Perahia, T. P. M. Alegre, A. H. Safavi-Naeini, and O. Painter, Appl. Phys. Lett. **95**, 201114 (2009).
[15] G. Björk, A. Karlsson, and Y. Yamamoto, Appl. Phys. Lett. **60**, 304 (1992).
[16] J. Rosenberg, Q. Lin, and O. Painter, Nature Photon. **3**, 478 (2009).
[17] R. M. Camacho, J. Chan, M. Eichenfield, and O. Painter, Opt. Express **17**, 15726 (2009).